Temperature, magnetic field, and field angular dependence of critical current of REBCO intermediate grown superconducting joint

OPEN ACCESS
IOP Publishing
Superconductor Science and Technology
Supercond. Sci. Technol. **38** (2025) 125003 (10pp)
https://doi.org/10.1088/1361-6668/ae1eaa

Temperature, magnetic field, and field angular dependence of critical current of REBCO intermediate grown superconducting joint

Y Takeda[1,*], G Nishijima[1], T Motoki[2], J Shimoyama[2] and H Kitaguchi[1]

[1] National Institute for Materials Science, 1-2-1 Sengen, Tsukuba, Ibaraki 305-0047, Japan
[2] Department of Physical Sciences, Aoyama Gakuin University, 5-10-1 Fuchinobe, Chuo-ku, Sagamihara, Kanagawa 252-5258, Japan

E-mail: TAKEDA.Yasuaki@nims.go.jp

Received 3 July 2025, revised 28 October 2025
Accepted for publication 12 November 2025
Published 3 December 2025

Abstract

Clarifying the critical current characteristics of high-temperature superconducting joints can contribute to the development of persistent-mode high-temperature superconducting magnets. We evaluated the temperature, magnetic field, and field angular dependence of the critical current of intermediate grown superconducting (iGS) joints formed between high-temperature superconducting $REBa_2Cu_3O_y$ (REBCO, RE = rare earth, $y \approx 7$) tapes. The critical currents were determined by performing current decay measurements on closed-loop samples, each containing an iGS joint. The temperature, magnetic field, and field angular dependence of the critical current of the iGS joints were found to be similar to that of commercially available REBCO tapes. The critical current characteristics of iGS joints can be described using models developed for the tapes. This similarity in the characteristics can contribute to the design of persistent-mode magnets using REBCO tapes.

Keywords: superconducting joint, high-temperature superconductor, angular dependence, persistent-mode magnet

1. Introduction

$REBa_2Cu_3O_y$ (REBCO, RE = rare earth, $y \approx 7$) is a promising high-temperature superconductor (HTS) that can be used to develop superconducting magnets generating very high magnetic fields at low temperatures, or magnets operated at higher temperatures. REBCO conductors are commercially available in the form of coated conductor tapes [1, 2]. These tapes have been used in the development of REBCO magnets intended for various applications, including magnetic resonance imaging [3], nuclear magnetic resonance (NMR) [4], maglev systems [5], generators [6], and fusion energy systems [7].

An HTS exhibits anisotropic electromagnetic properties. The critical current (I_c) of a REBCO tape depends on the direction of the applied magnetic field. Superconducting magnets made of REBCO tapes have been designed considering this anisotropy, that is, the field angular dependence of I_c [8–11]. To accommodate such designs, REBCO tapes have been characterized considering the dependence of I_c not only on the temperature and magnetic field strength but also on the field angle [1, 8, 12].

Despite the challenges in achieving superconducting joints between HTS conductors, Park *et al* successfully fabricated a superconducting joint between REBCO tapes [13]. Since

* Author to whom any correspondence should be addressed.

this pioneering work, various research groups have developed REBCO superconducting joints [14–19]. One of the most promising methods for fabricating such joints is the intermediate grown superconducting (iGS) joint technique, which adopts a joining strap [16]. The REBCO layers of the tapes are connected to the joining strap via an epitaxially grown REBCO intermediate layer. Existing papers report a high I_c of the joint (I_{cj}) and a low joint resistance of less than 10^{-13} Ω [16, 20, 21]. A REBCO coil connected at both ends with iGS joints was fabricated and combined as an insert in a 400 MHz NMR magnet. This demonstrates that iGS joints are applicable to persistent-mode NMR magnets [20].

The in-field I_{cj} characteristics of several types of REBCO superconducting joints have been reported at various temperatures [20, 22, 23]. In these studies, the magnetic field was either perpendicular or parallel to the surface of the joined tape. However, in practice, the direction of the magnetic field applied to the superconducting joints in a magnet is not necessarily perpendicular or parallel. Since the current in the iGS joint must flow along the *c*-axis of REBCO, the angular dependence of I_{cj} may not be as simple as that of I_c of the tape.

In addition, the reported I_{cj} values of various REBCO superconducting joints were evaluated through transport measurements, similar to the I_c measurement of a superconducting tape/wire, with a voltage criterion on the order of 10^{-6} V. The voltage of 10^{-6} V corresponds to the joint resistance of 10^{-8} Ω at 100 A. This resistance is too high for a persistent current to flow.

We developed $(Bi,Pb)_2Sr_2Ca_2Cu_3O_y$ (Bi-2223) HTS joints and investigated the I_{cj} characteristics of Bi-2223 closed-loop samples using current decay measurements [24]. This measurement method enabled the evaluation of I_{cj} with a low-voltage criterion (V_c) of 10^{-8} V. This I_{cj} value is comparable to the maximum current at which an iGS joint can exhibit a low resistance. Our previous study suggested that a joint resistance of 10^{-12} Ω could be achieved at a current of about 0.8 times I_{cj} ($V_c = 10^{-8}$ V) [25]. In addition, by applying a magnetic field to the joint in various directions, we evaluated the field angular dependence of I_{cj} [24].

To appropriately design REBCO persistent-mode magnets, the I_{cj} characteristics of the iGS joints with a low-voltage criterion should be investigated in detail. In this study, we evaluated I_{cj} of REBCO closed-loop samples with an iGS joint. The temperature, magnetic field, and field angular dependence of I_{cj} in the iGS joints are discussed. This study contributes to a better understanding of the underlying materials science involving REBCO superconducting joints.

2. Method

Two one-turn closed-loop samples, designated as #A and #B, were prepared, each containing an iGS joint. Figures 1(a) and (b) show a schematic of the sample and a schematic of the magnified view of the iGS joint, respectively. The loop diameter was 100 mm. The self-inductance (L) of the samples was 0.47 μH.

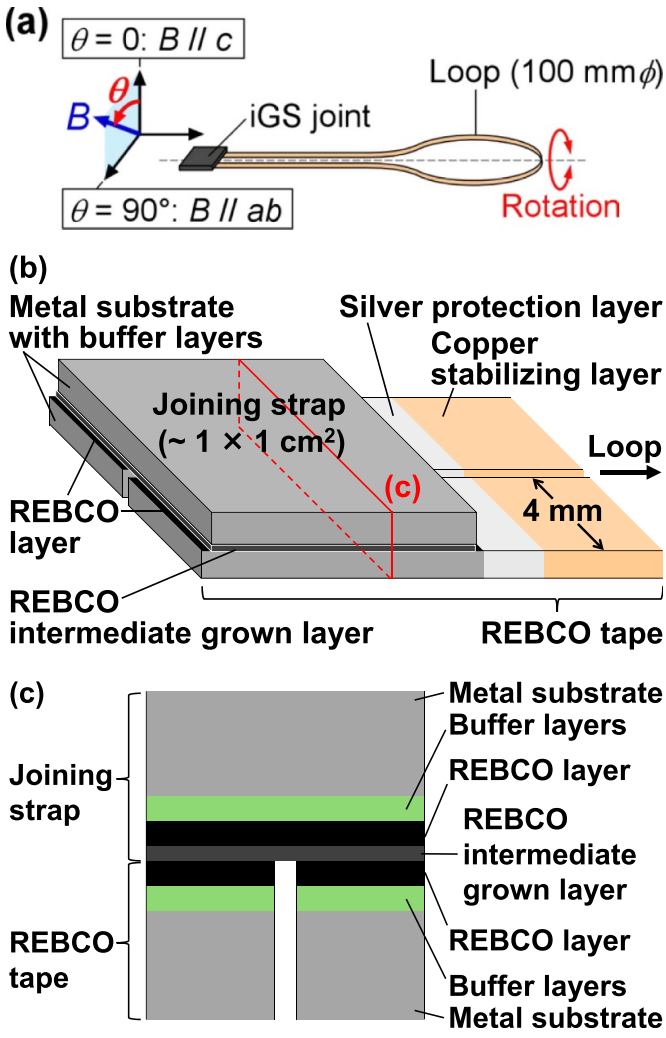

Figure 1. (a) Schematic of a one-turn closed-loop sample, along with the definition of the magnetic field angle (θ). The magnetic field (B) is applied only to the iGS joint. (b) Schematic of a magnified view of the iGS joint. (c) Cross-sectional view (not to scale) of the joint structure. The position is shown in (b).

To prepare the sample, a 1 m-long and 4 mm-wide REBCO tape was used. I_c of the tape at 77 K in the self-field was 280 A, as evaluated by transport measurements under an electric field criterion of 10^{-6} V cm^{-1}. Both ends of the tape were connected via an iGS joint. Figure 1(c) shows a cross-sectional view (not to scale) of the joint structure. The copper stabilizing layer and silver protection layer at both ends were removed by chemical etching. The intermediate layer was epitaxially grown using the joining strap with a microcrystalline REBCO film. After a heat treatment with pressure and oxygen annealing, the iGS joint was formed [14, 16]. This joining process does not cause severe degradation of the tape. A persistent current with a low resistance was observed in closed-loop samples [21, 25]. For the iGS joints, every effort was made to ensure that the area of the REBCO layer exposed to the environment was as small as possible.

The sample was placed in a previously developed joint resistance evaluation system [26]. We carefully fixed the samples to avoid degradation, using the handling method established

in our previous study [21]. The angle of the magnetic field (θ) was defined as shown in figure 1(a). The magnetic field direction at $\theta = 0$ was perpendicular to the surface of the joining strap, that is, parallel to the *c*-axis of REBCO. We applied the magnetic field only to the joint and rotated the sample around the central axis, as indicated by the gray dashed line in the figure. This enables the control of the magnetic field angle [24].

The I_{cj} values were evaluated in the temperature (T) and magnetic field (B) ranges of 4–77 K and 0.1–2.0 T, respectively, under various field angles. Using the evaluation system, we introduced a current into the closed-loop sample. The decay of the introduced loop current (I_{loop}), that is, the time (t) dependence of I_{loop}, was measured at a sampling rate of 1 Hz. From the obtained I_{loop}–t curve, the I_{loop} dependence of the voltage (V) was calculated using $V = -L\Delta I_{loop}/\Delta t$. The V–I_{loop} was smoothed using a 25-point moving average. The I_{cj} value was determined at a voltage criterion (V_c) of 10^{-8} V using the smoothed V–I_{loop} curve at voltages ranging from 4×10^{-9}–2×10^{-8} V. To estimate the I_{cj} values by extrapolation, some of the smoothed V–I_{loop} curves were fitted to an empirical power law model ($V \propto {I_{loop}}^n$, where n is a constant) using the least-squares method. The details of the evaluation system, including the I_{loop} measurements, and the I_{cj} evaluation method are described in [21, 24], respectively.

Table 1 shows the I_{cj} and n values of the samples #A and #B at 77 K in the self-field, as evaluated using the method described in the previous paragraph. The n value was evaluated in the voltage range of 0.5–2 $\times 10^{-8}$ V. Sample #A exhibited a higher self-field I_{cj} than sample #B. In contrast, the n values for the samples were comparable. Note that the same fabrication process for the iGS joint, as described in [16], was applied to both #A and #B. No artificial pinning centers were introduced into the REBCO of the iGS joints.

3. Results and discussion

3.1. Temperature dependence

Figure 2 shows the temperature dependence of I_{cj} in samples #A and #B at $\theta = 0$ (B // c), 45°, and 75° in the magnetic field range of 0.5–1.5 T. We did not evaluate the high I_{cj} values for #A at low temperatures or high fields. There are two main reasons for this. First, there is an upper limit of the initial I_{loop} value that can be introduced into the sample using our evaluation system [24]. Another reason is that introducing a high I_{loop} may mechanically degrade the superconducting joint located in the magnetic field due to the electromagnetic force.

Similar to the self-field I_{cj} shown in table 1, a higher I_{cj} was observed in #A than in #B at 0.5 T and in the 0–75° range. I_{cj} for both #A and #B increased with decreasing temperature under the same magnetic field and angle. Regardless of the strength and angle of the magnetic field, the increase in I_{cj} appears to be exponential at temperatures below 50 K in both #A and #B. Such an exponential increase is generally observed in the temperature dependence of the critical current density (J_c) for REBCO tapes below 50 K [27–29]. Considering the near-single-crystal texture of REBCO in an iGS joint similar to that in a tape [16, 30], the exponential temperature dependence of J_c for the tapes can be applied to I_{cj} as follows:

$$I_{cj}(T,B,\theta) = I_{cj}(T=0,B,\theta)\exp(-T/T^*), \quad (1)$$

where T^* is a parameter related to the number of defects that act as effective pinning centers. From the I_{cj}–T curves in the temperature range of 20–50 K, we evaluated T^* for samples #A and #B using (1). Figure 3 shows the angular dependence of T^* for #A and #B. Sample #A showed a lower T^* than sample #B. This implies that there were more pinning defects in #A than in #B. The T^* values were in the temperature range of 19.7–35.9 K, which were comparable to those reported for various REBCO tapes (14–36 K) in the magnetic field range of 0–2 T [27–29].

We compared the field dependence of T^* for the iGS joint with that for REBCO tapes. Figure 4 shows the field dependence of T^* in the angle range of 0–80° for #A. The field dependence can be divided into three angular regions. In the low-angle region of 0–45°, T^* was independent of the field, although a slight decrease in T^* was observed with the increasing angle. In contrast, at high angles of 75° and 80°, T^* decreased with increasing field strength. An intermediate behavior was observed at 60°, which corresponds to the intermediate region.

The field dependence of T^* for the iGS joint is similar to that reported for various REBCO tapes [27, 29]. In the field range of 0–2 T, the T^* value for REBCO tapes is independent of the field at θ values of 0 and 45°, whereas it decreases with increasing field at 90°. It is suggested that the I_{cj} for the iGS joint depends exponentially on the temperature below 50 K, similar to J_c for REBCO tapes.

3.2. Magnetic field dependence

Figure 5 shows the magnetic field dependence of I_{cj} at 77 K and 0–90° for #A and #B. In both the samples, I_{cj} at $\theta = 0$ (B // c) was lower than that at 90° (B // ab). This is consistent with the anisotropy of I_{cj} for iGS joints reported previously [20].

I_{cj} for both #A and #B decreased with the increasing field. Generally, the field dependence of J_c for REBCO tapes can be divided into three regimes: a low-field regime where J_c is nearly independent of the field; an intermediate-field regime with a power-law decrease in J_c; and a high-field regime where J_c drops sharply [27, 31]. REBCO superconducting joint samples, which are not the iGS joints, are known to exhibit a field dependence for I_{cj} in the three regimes [23]. As shown in figure 5, the field dependence of I_{cj} in #A and #B at 77 K can be classified into the low- or intermediate-field regimes.

In the intermediate-field regime at about 1 T, the power law $J_c \propto B^{-\alpha}$, where α is a fitting parameter, is generally used for REBCO tapes [27, 32–34]. In the magnetic field range of 0.5–1.5 T, the power law can be applied to I_{cj}–B. We calculated α for #A in the temperature range of 35–77 K and for #B at 77 K using $I_{cj} \propto B^{-\alpha}$ in the field range of 0.5–1.5 T.

Figure 6 shows the angular dependence of α for #A and #B. Random pinning is effective in REBCO tapes with α of

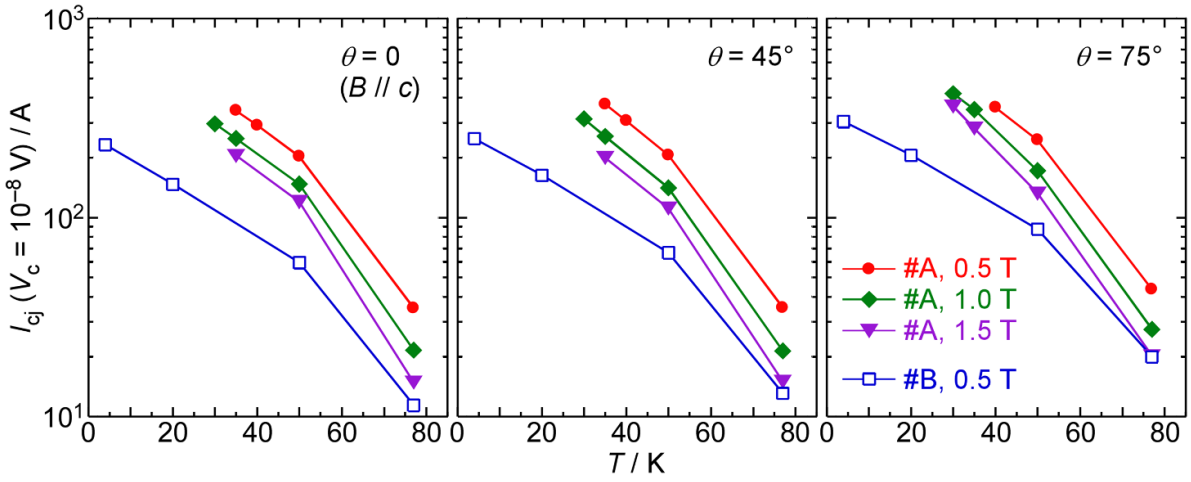

Figure 2. Temperature dependence of I_{cj} in samples #A and #B at $\theta = 0$, 45°, and 75° and in the magnetic field range of 0.5–1.5 T. I_{cj} exponentially increases with decreasing temperature below 50 K. At temperatures ranging from 20 to 50 K, the exponential temperature dependence of I_{cj} described in equation (1) is applicable.

Table 1. Self-field I_{cj} ($V_c = 10^{-8}$ V) and n values (obtained at 0.5–2 × 10^{-8} V) of the tested REBCO closed-loop samples at 77 K.

Sample	I_{cj} (A)	n (–)
#A	108	36
#B	47.5	35

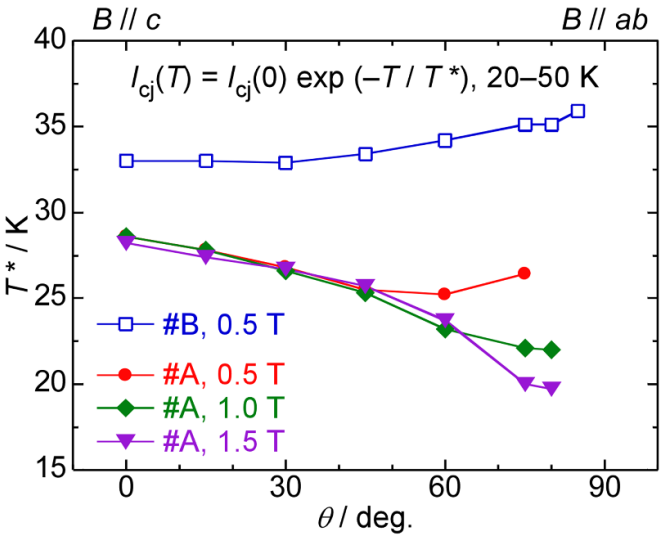

Figure 3. Angular dependence of T^* in samples #A and #B in the magnetic field range of 0.5–1.5 T. Sample #A shows a lower T^* than sample #B, implying that it contains more pinning defects than #B.

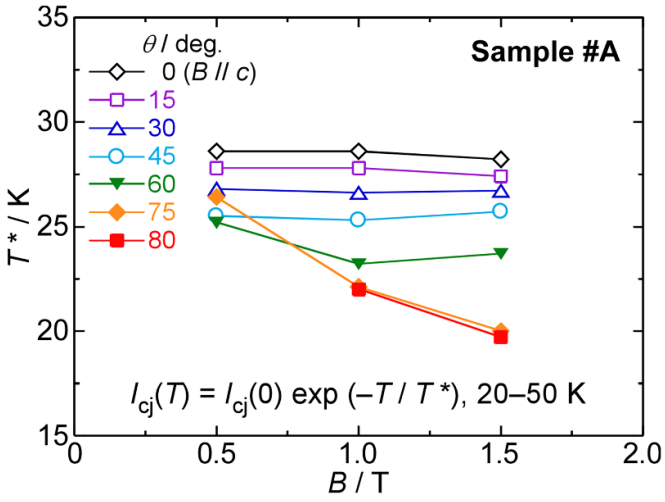

Figure 4. Field dependence of T^* in sample #A in the angle range of 0–80°, which can be divided into three angular regions: low-angle region (0–45°), intermediate-angle region (60°), and high-angle region (75–90°). The similar field dependence has been reported for various REBCO tapes.

about 0.5 [32, 33]. In the temperature and angle ranges of 35–50 K and 0–75°, respectively, the α value for #A was about 0.5, where random pinning is probably the dominant pinning mechanism. The decrease in α close to 90° is due to the *ab*-plane correlated pinning centers [32]. In contrast, α for #A and #B was higher at 77 K. It is reported that α increases as the effectiveness of the *c*-axis correlated pinning centers weakens, particularly at high temperatures [34]. This explains the higher α value observed at 77 K. At low angles, #B showed higher α than #A at 77 K. This implies that #B contained fewer *c*-axis correlated pinning centers than #A.

We compared the temperature dependence of α for #A with that for REBCO tapes. Figure 7 shows the temperature dependence of α for #A in the angle range of 0–90°. Similar to the field dependence of T^* shown in figure 4, the temperature dependence of α can be divided into three angular regions. In the low-angle range of 0–45°, α was largely independent of the temperature in the range of 35–50 K, though it slightly increased from 0.47 to 0.56 with increasing angle. In the 0–45° and 50–77 K ranges, α increased with increasing temperature. In contrast, in the 60–80° range, α increased linearly with the increasing temperature from 35 K to 77 K. The temperature dependence at 80° was stronger than that at 60° and 75°. At

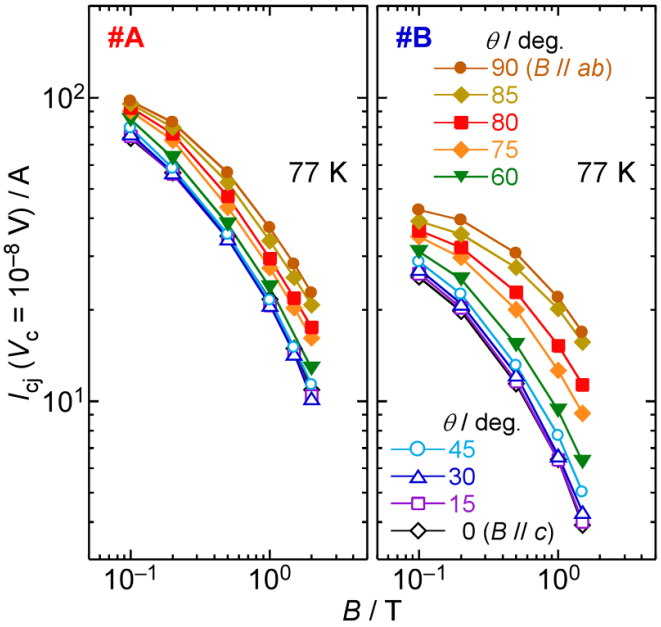

Figure 5. Field dependence of I_{cj} in samples #A and #B at 77 K and 0–90°. This can be classified into low- or intermediate-field regime, which is used in the division of the field dependence of J_c for REBCO tapes. In the intermediate-field regime of 0.5–1.5 T, the power law $I_{cj} \propto B^{-\alpha}$ can be applied.

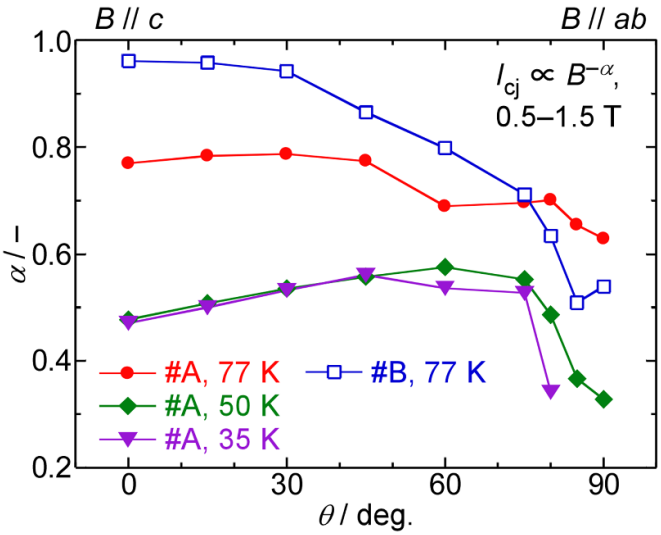

Figure 6. Angular dependence of α in the temperature range of 35–77 K for #A and #B. The decrease in α close to 90° is due to the *ab*-plane correlated pinning centers. The higher α values at 77 K can be attributed to the weakening of the effectiveness of *c*-axis correlated pinning centers.

50 K, the lower α values of 0.33 and 0.37 were observed at 85° and 90°, respectively, than those in the 0–80° range (0.48–0.58). These results imply that α exhibits a strong temperature dependence in the high-angle range of 80–90° from low to high temperatures. This corresponds to a decrease in α close to 90° shown in figure 6, which is due to the *ab*-plane correlated

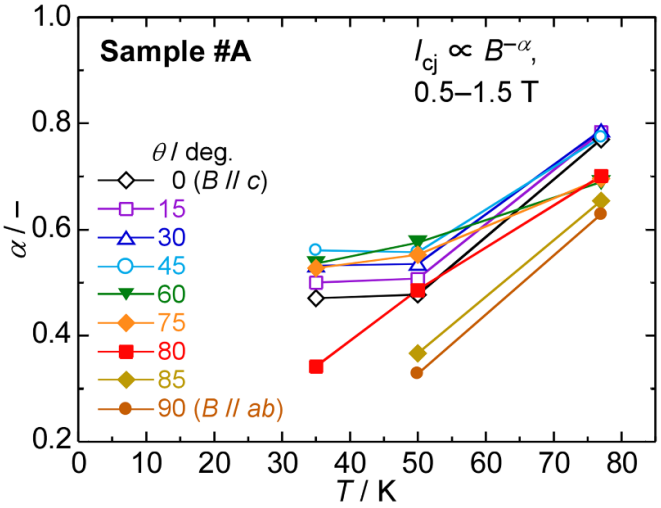

Figure 7. Temperature dependence of α in the angle range of 0–90° in sample #A, which can be divided into three angular regions, similar to the field dependence of T^* shown in figure 4. The similar temperature dependence of α for various REBCO tapes is reported.

pinning centers. The temperature dependence in the 60–75° range can be classified into the intermediate-angle region.

The temperature dependence of α for the iGS joint is similar to that reported for various REBCO tapes [27, 33]. For REBCO tapes, α is largely independent of the temperature below 50 K at θ values of 0 and 45°, while it increases with increasing temperature above 20 K at 90°. It is suggested that the I_{cj} for the iGS joint depends on the field with a power law in the intermediate-field regime, similar to J_c for REBCO tapes.

3.3. *Field angular dependence*

Figure 8 shows the field angular dependence of I_{cj} in samples #A and #B in the temperature range of 4–77 K and in the field strength range of 0.1–2.0 T, where the symbols indicate the experimentally obtained values. At 4, 20, and 35 K, the I_{cj} values close to 90° are missing due to the upper limit of the initial I_{loop} value and avoiding a large electromagnetic force. Figure 8 shows all the evaluated I_{cj} data points for #B. Regardless of the field and temperature, I_{cj} for both #A and #B exhibited a peak at 90° (*B // ab*). This peak is generally observed in the angular dependence of J_c for REBCO tapes without artificial pinning centers [12, 35].

In the 1.0–2.0 T range and at $\theta = 0$, a small peak for I_{cj} was observed in #A. This peak is typically observed in the angular dependence of J_c for an undoped REBCO film [36]. This is due to *c*-axis correlated defects, such as twin boundaries or stacking faults. Considering the near-single-crystal texture in an iGS joint [16, 30], the same pinning mechanism is applicable. It is suggested that the *c*-axis correlated defects acted as effective pinning centers in #A. This is consistent with the discussion in section 3.2: There are fewer *c*-axis correlated pinning centers in #B. This is because no I_{cj} peak was observed at $\theta = 0$ in #B.

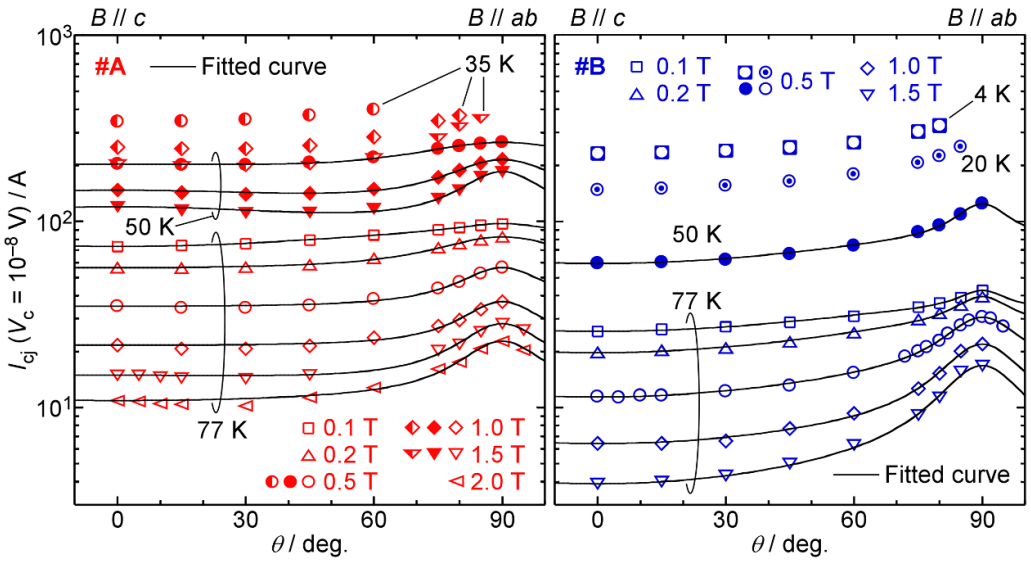

Figure 8. Angular dependence of I_{cj} in samples #A and #B in the temperature range of 4–77 K and the magnetic field strength range of 0.1–2.0 T. Symbols indicate the experimentally obtained values. Black solid curves are the fitted curves at 50 and 77 K obtained using equations (2) and (3). Regardless of the field and temperature, I_{cj} for both #A and #B shows a peak at 90°. Although equations (2) and (3) are proposed for a REBCO tape, the I_{cj}–θ fitted curves are in good agreement with the experimentally obtained values.

Given that the angular dependence of I_{cj} for both #A and #B was similar to that of J_c for REBCO tapes, the I_{cj}–θ data were fitted using the I_c model for the tapes. We fitted the I_{cj}–θ data at 50 and 77 K, where the I_{cj} ($\theta = 90°$) values were obtained. The black solid curves in figure 8 are the fitted curves obtained using equations (2) and (3), as follows [37]:

$$I_{cj}(T,B,\theta) = a_1 f_1(\omega_1(T,B),\theta) + a_2 f_2(\omega_2(T,B),\theta),$$

$$\begin{cases} f_1(\omega_1,\theta) = \frac{1}{\omega_1{}^2\cos^2\theta+\sin^2\theta} \\ f_2(\omega_2,\theta) = \frac{1}{\sqrt{\cos^2\theta+\omega_2{}^2\sin^2\theta}} \end{cases} \quad (2)$$

$$\begin{pmatrix} a_1 \\ a_2 \end{pmatrix} = \frac{\omega_1{}^2\omega_2}{1-\omega_1{}^2\omega_2} \begin{bmatrix} \omega_2{}^{-1} & -1 \\ -1 & \omega_1{}^{-2} \end{bmatrix} \begin{pmatrix} I_{cj}(\theta=0) \\ I_{cj}(\theta=90°) \end{pmatrix}. \quad (3)$$

The fitting parameters ω_1 and ω_2 are the peak sharpness parameters. Equations (2) and (3) describe the angular dependence of I_c for a commercially available REBCO tape [37]. The excellent fit shown in figure 8 indicates that the angular dependence of I_{cj} for the iGS joints can be described using the model for the REBCO tape.

Figure 9 shows the magnetic field dependence of the fitting parameters ω_1 and ω_2 for #A and #B at 50 and 77 K. The figure suggests that ω_1 for both #A and #B depends on the magnetic field and probably converges to about 5 with increasing field strength. In contrast, ω_2 is largely independent of the magnetic field. The variation in ω_2 (0.67–1.21) was lower than that in ω_1 (2.30–8.30). The lower variation in ω_2 has also been reported for the fitted I_{cj}–θ curves of a REBCO tape [38].

Equation (2) shows that f_2 is concave upward with $\omega_2 > 1$. The term $a_2 f_2$ in (2) has little effect on the sharpness of the I_{cj} peak at 90° with $\omega_2 \gtrsim 1$. The peak sharpness is in turn mainly determined by the term $a_1 f_1$. Equation (2) also shows that with

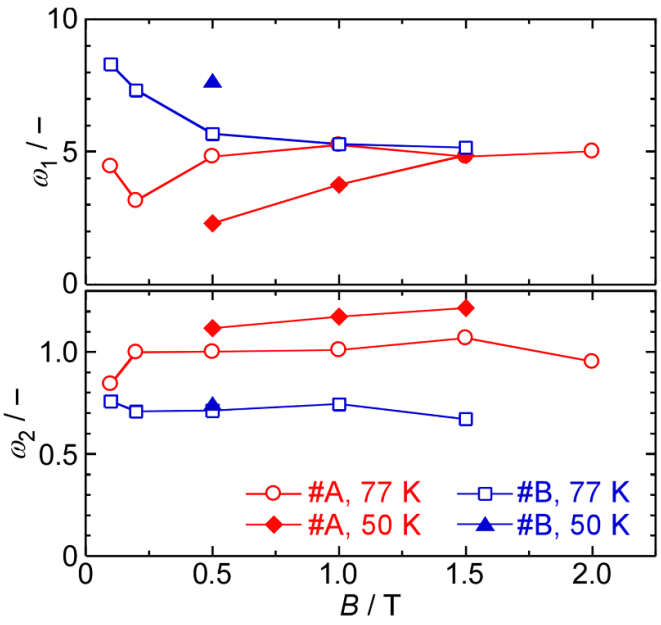

Figure 9. Field dependence of the fitting parameters ω_1 and ω_2 in equations (2) and (3) for samples #A and #B at 50 and 77 K. It is suggested that ω_1 depends on the field and probably converges to about 5 with increasing field strength. In contrast, ω_2 is largely independent of the field and its variation is lower than that of ω_1.

$\omega_1 > 1$, the greater the ω_1 value, the sharper the peak of f_1 at 90°. An increase in ω_1 with increasing field was observed in #A at 50 K with ω_2 in the range of 1.12–1.21. This increase in ω_1 corresponds to the peak sharpening of I_{cj}.

To evaluate the sharpness of the I_{cj} peak at 90°, we calculated the full width at half maximum (FWHM) of the peak using the fitted I_{cj}–θ curves shown in figure 8. Figure 10 shows the magnetic field dependence of the FWHM for #A and #B

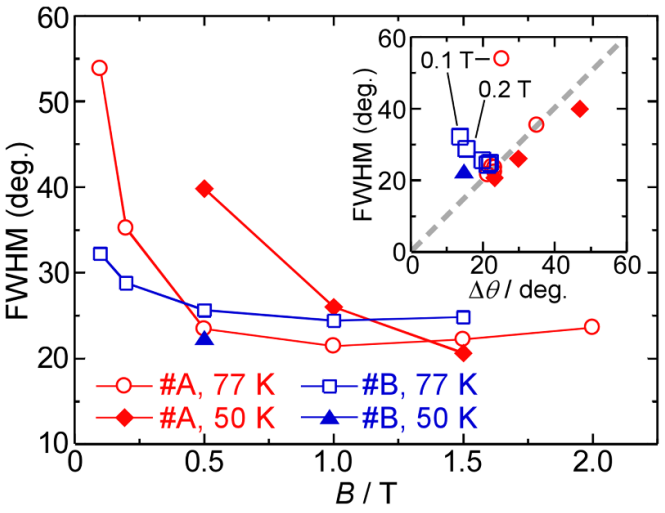

Figure 10. Field dependence of FWHM in samples #A and #B at 50 and 77 K. FWHM decreases with the applied field and converges to a range of 20–25° above 1 T. Inset shows the relationship between FWHM and $\Delta\theta$ defined by equation (4). The gray dashed line corresponds to FWHM $= \Delta\theta$. Most of the data points are in the vicinity of this line, suggesting that the I_{cj} peak at 90° can be interpreted by Long's model.

at 50 and 77 K. The FWHM decreases with increasing field and converges to a range of 20–25° above 1 T. Long reported that the effectiveness of *c*-axis correlated pinning centers increases at low fields in a REBCO tape, resulting in peak broadening [35]. This is consistent with the field dependence of the FWHM, as shown in figure 10. A decrease in the FWHM with increasing field was observed for #A at 50 K. This corresponds to the peak sharpening of I_{cj} with an increase in ω_1 described above.

We physically interpret the relationship between ω_1 and the FWHM. Long proposed a physical model to explain the angular dependence of J_c in a REBCO tape [35]. The model assumes that the pinned vortex path can be described as a directed random walk along defects. The relationship $J_c \propto \left(\cos^2\theta + {\Gamma_2}^2\sin^2\theta\right)^{-1}$ is proposed, where Γ_2 is the peak sharpness parameter. The parameter Γ_2 has a physical meaning associated with the random walk and is inversely proportional to the average spacing of *c*-axis correlated defects.

As described above, from equation (2), the peak sharpness is mainly determined by the term $a_1 f_1$ with $\omega_2 \gtrsim 1$. In this case, $I_{cj} \propto \left(\cos^2\theta + {\omega_1}^{-2}\sin^2\theta\right)^{-1}$ is applicable to describe the peak at 90°. This means that ${\omega_1}^{-1}$ is probably consistent with Γ_2 in Long's model. Here, we assume $I_{cj} \propto \left(\cos^2\theta + {\omega_1}^{-2}\sin^2\theta\right)^{-1}$ to describe the peak at 90°. The FWHM for the peak ($\Delta\theta$) is calculated as follows:

$$\Delta\theta = 2\arcsin\frac{1}{\sqrt{{\omega_1}^2+1}}. \qquad (4)$$

The inset in figure 10 shows the relationship between $\Delta\theta$ and FWHM for #A and #B at 50 and 77 K and in the field strength range of 0.1–2.0 T. The gray dashed line corresponds to FWHM $= \Delta\theta$.

Most of the data points are near the dashed line. This suggests that the above assumption is correct for these data points, meaning that ${\omega_1}^{-1}$ is consistent with Γ_2 in Long's model. At 77 K and in the 0.5–2 T range, Γ_2 is reported to range from 0.09 to 0.22 [35], which is comparable to the ${\omega_1}^{-1}$ range of 0.18–0.21. Thus, at most temperatures and magnetic fields, the peak of I_{cj} at 90° can be interpreted using Long's model. This implies that ${\omega_1}^{-1}$ has the same physical meaning as Γ_2. The ω_1 value of about 5 at 77 K and field strength range of 0.5–2 T for both #A and #B may suggest that the average spacing of the effective *c*-axis correlated defects is similar in both the joints, which were fabricated using the same fabrication process.

The data points at 77 K under 0.1 T (#A) and 0.1–0.2 T (#B) are far from the dashed line. Under these conditions, the I_{cj} peak at 90° was relatively heavy-tailed. This makes it difficult to describe the peak using f_1. From equation (2), f_2 with $\omega_2 < 1$ is concave downward and influences the peak shape. Considering the heavy-tailed peaks with $\omega_2 < 1$ in these data points, the FWHM was determined by both f_1 and f_2. This resulted in data points that were far from the dashed line. Note that f_2 is also used to express the J_c peak at 90° for REBCO tapes, particularly when random pinning is effective [39–41]. This probably corresponds to the fact that heavy-tailed peaks are observed at low fields in the field strength range of 0.1–0.2 T.

I_{cj} of the iGS joints depends on the magnetic field angle, similar to J_c of REBCO tapes. The I_{cj} peak at 90° can be physically interpreted at most temperatures and magnetic fields using Long's model to explain the J_c peak for the tape [35].

3.4. Discussion

As discussed in sections 3.1–3.3, our results suggest that the $I_{cj}(T, B, \theta)$ characteristics of the iGS joint are similar to the $J_c(T, B, \theta)$ characteristics of the REBCO tapes. This finding can contribute to the design of persistent-mode REBCO magnets using iGS joints. Because I_{cj} is noticeably lower than I_c for REBCO tapes, the iGS joints should be placed in a low-field area and the surface of the joining strap should be nearly parallel to the magnetic field, that is, B // ab.

The critical current ratio (CCR: I_{cj} divided by wire I_c) is occasionally used to compare the performance of a superconducting joint with that of the virgin wire [42]. We attempted to estimate the rough CCR at 77 K in the self-field using the I_{cj} ($V_c = 10^{-8}$ V) values. I_c of the tape (I_c^{tape}) at 10^{-8} V cm^{-1} can be extrapolated to be 220 A from that at 10^{-6} V cm^{-1} (280 A), assuming that a typical n value of 20 [2] is constant at electric fields lower than 10^{-6} V cm^{-1}. The rough CCR values were estimated to be 49% for #A and 21% for #B. These CCR values appear to indicate the joint performance compared with the virgin tape. However, I_c^{tape} at 10^{-8} V cm^{-1} would be underestimated due to higher n values at lower electric fields [43]. In addition, for the proper calculation of CCR, I_{cj} and I_c^{tape} must be determined using the same criterion of the voltage or electric field. The estimated rough CCR values have little quantitative meaning. They are merely a qualitative indicator showing that the performance of the iGS joint is still lower than that of the virgin tape.

The similarity in the characteristics of the iGS joint to those of the REBCO tapes is contrary to our initial expectation. Although the entire assembly of the iGS joint is REBCO, the current in the joint must flow along the *c*-axis. This is a considerable difference compared with a tape, in which the *ab*-plane transport should determine I_c. The *c*-axis transport properties in HTS materials have been an interesting topic of discussion [44]. The clarification of the I_{cj} characteristics of the iGS joint will contribute to this discussion of the *c*-axis transport.

From this study, however, it is difficult to clarify whether I_{cj} is determined by J_c parallel to the *ab*-plane ($J_c^{//ab}$) or *c*-axis ($J_c^{//c}$) at the joint. Considering the similarity in the characteristics of the iGS joint to those of the REBCO tapes, it is possible that $J_c^{//ab}$ at the joint contributes significantly to I_{cj}. However, previous studies have suggested that I_{cj} is determined by $J_c^{//c}$ at the joint [16, 20]. Jia *et al* reported that $J_c^{//c}$ at 90° (B // ab) is higher than that at $\theta = 0$ (B // c) for a REBCO tape [45]. This implies that the angular dependence of $J_c^{//c}$ is similar to that of $J_c^{//ab}$ for the REBCO tape. Considering this angular dependence, it is possible that $J_c^{//c}$ at the joint contributes significantly to I_{cj}. Further studies are needed to clarify the contribution of $J_c^{//ab}$ and $J_c^{//c}$ to I_{cj}.

Sample #B exhibits a lower I_{cj} value than sample #A. This difference in I_{cj} cannot be attributed to the effective joint area but to the effective pinning centers. This is because #B has fewer *c*-axis correlated pinning centers, such as twin boundaries [36]. It is possible that the insufficient oxygen supply in #B, which is due to the formation of an intermediate grown layer that requires longer time for oxygen diffusion, resulted in fewer twin boundaries and a lower I_{cj}. The intermediate grown layer in #B may contain a small number of grain boundaries, which act as oxygen diffusion paths [16]. Microstructural analyses, including lattice constant evaluations and microstructural observations, will help verify this assumption. The lattice constants evaluated by x-ray diffraction measurements will determine the average oxygen content of the joints. The distribution of oxygen content may be clarified by measuring local critical temperatures using magneto-optical imaging or magnetic microscopy. The microstructural observations will reveal the presence of *c*-axis correlated defects in the joints, such as twin boundaries or stacking faults.

In a preliminary experiment, we observed the variation in I_{cj} in four closed-loop samples, including #A and #B, although the same fabrication process for the iGS joint [16] was applied. The four samples showed the I_{cj} ($V_c = 10^{-8}$ V) values of 40.6, 47.5, 88.5, and 108 A at 77 K in the self-field, respectively. There is room for improving the reproducibility of fabricating an iGS joint. This may be due to the mechanical pressure during heat treatment, the quality of the REBCO layer of tapes, and the tape thickness are not uniform. Also, the oxygen content is one of the dominant factors affecting I_{cj}, as described in the previous paragraph. It is necessary to clarify the effect of various factors on I_{cj}. This will contribute to improving the fabrication reproducibility.

One of the promising methods to increase I_{cj} reproducibly is the introduction of effective pinning centers into an iGS joint. This may also lead to achieving a flatter angular dependence of I_{cj}. We studied the introduction of $BaMO_3$ (M = Sn, Zr, Hf) nanoparticles and $Ba_2Cu_3O_4X_2$ (X = Cl, Br) precipitates as pinning centers into REBCO films fabricated using the metal-organic deposition (MOD) process [46–48]. Our previous studies have reported that the $Ba_2Cu_3O_4X_2$ precipitates not only promote epitaxial growth of the REBCO layer at lower temperatures but also act as *c*-axis correlated pinning centers. Given that an iGS joint is fabricated using a similar MOD process [14, 16], these secondary phases may serve as effective pinning centers. We plan to fabricate iGS joints with these secondary phases introduced.

To contribute to the discussion of the *c*-axis transport properties in HTS materials and improve the reproducibility of the fabrication, the bottleneck in the iGS joint where I_{cj} is dominant should be clarified. The iGS joint contains three layers of REBCO: REBCO in the joined tapes, REBCO in the joining strap, and an intermediate grown layer [16]. The current flowing through the iGS joint passes through three REBCO layers and four joining interfaces. We plan to analyze each REBCO film in the joined tapes, joining strap, and intermediate grown layer. Further studies can consider the dominant factors affecting I_{cj} for the iGS joint. This can help to more comprehensively understand the materials science involved in HTS joints.

4. Conclusion

In this study, the temperature, magnetic field, and field angular dependence of I_{cj} ($V_c = 10^{-8}$ V) in iGS joints was discussed. The I_{cj} characteristics of these joints were found to be similar to the J_c characteristics of commercially available REBCO tapes. The temperature, field, and angular dependence of I_{cj} can be described using models developed for REBCO tapes. I_{cj} depends exponentially on the temperature, on the magnetic field strength with a power law in the intermediate-field regime and on the angle, which shows a peak in the field parallel to the *ab*-plane. The similarity between the characteristics of the iGS joint and REBCO tapes can contribute to the design of persistent-mode magnets using REBCO tapes.

Data availability statement

All data that support the findings of this study are included within the article (and any supplementary files).

Acknowledgment

This work was supported by JST Mirai-Program Grant Numbers JPMJMI17A2 and JSPS KAKENHI Grant Number JP22K14482, Japan. The authors would like to thank Dr M. Hamada of Japan Superconductor Technology, Inc. and Dr K. Ohki of Sumitomo Electric Industries, Ltd for providing the samples.

ORCID iDs

Y Takeda 0000-0001-7217-9853
G Nishijima 0000-0001-7493-0559
T Motoki 0000-0003-3218-0977
J Shimoyama 0009-0007-1783-676X

References

[1] Uglietti D 2019 A review of commercial high temperature superconducting materials for large magnets: from wires and tapes to cables and conductors *Supercond. Sci. Technol.* **32** 053001
[2] Godeke A 2023 High temperature superconductors for commercial magnets *Supercond. Sci. Technol.* **36** 113001
[3] Yokoyama S *et al* 2020 Design and cooling properties of high stable field REBCO superconducting magnet for MRI *IEEE Trans. Appl. Supercond.* **30** 4400904
[4] Bruker Corporation 2020 Successful installation of world's first 1.2 GHz NMR system enables novel functional structural biology research (available at: www.bruker.com/ja/news-and-events/news/2020/successful-installation-of-worlds-first-12-ghz-nmr-system-enables-novel-functional-structural-biology-research.html) (Accessed October 2025)
[5] Mizuno K, Sugino M, Tanaka M and Ogata M 2016 Experimental production of a real-scale REBCO magnet aimed at its application to maglev *IEEE Trans. Appl. Supercond.* **27** 3600205
[6] Bergen A *et al* 2019 Design and in-field testing of the world's first ReBCO rotor for a 3.6 MW wind generator *Supercond. Sci. Technol.* **32** 125006
[7] Zachary S *et al* 2024 The SPARC toroidal field model coil program *IEEE Trans. Appl. Supercond.* **34** 0600316
[8] Uglietti D, Kitaguchi H, Choi S and Kiyoshi T 2009 Angular dependence of critical current in coated conductors at 4.2 K and magnet design *IEEE Trans. Appl. Supercond.* **19** 2909–12
[9] Kiyoshi T, Choi S, Matsumoto S, Zaitsu K, Hase T, Miyazaki T, Hamada M, Hosono M and Maeda H 2011 Bi-2223 innermost coil for 1.03 GHz NMR magnet *IEEE Trans. Appl. Supercond.* **21** 2110–3
[10] Matsumoto S, Kiyoshi T, Otsuka A, Hamada M, Maeda H, Yanagisawa Y, Nakagome H and Suematsu H 2012 Generation of 24 T at 4.2 K using a layer-wound GdBCO insert coil with Nb_3Sn and Nb–Ti external magnetic field coils *Supercond. Sci. Technol.* **25** 025017
[11] Nishijima G, Kitaguchi H, Tsuchiya Y, Nishimura T and Kato T 2013 Transport critical current measurement apparatus using liquid nitrogen cooled high-Tc superconducting magnet with variable temperature insert *Rev. Sci. Instrum.* **84** 015113
[12] Tsuchiya K *et al* 2016 Critical current characterization of commercial REBCO coated conductors at 4.2 and 77 K *IEEE Trans. Appl. Supercond.* **27** 6600205
[13] Park Y, Lee M, Ann H, Choi Y H and Lee H 2014 A superconducting joint for $GdBa_2Cu_3O_{7-\delta}$-coated conductors *NPG Asia Mater.* **6** e98
[14] Takeda Y, Maeda H, Ohki K and Yanagisawa Y 2022 Review of the temporal stability of the magnetic field for ultra-high field superconducting magnets with a particular focus on superconducting joints between HTS *Supercond. Sci. Technol.* **35** 043002
[15] Jin X, Yanagisawa Y, Maeda H and Takano Y 2015 Development of a superconducting joint between a $GdBa_2Cu_3O_{7-\delta}$-coated conductor and $YBa_2Cu_3O_{7-\delta}$ bulk: towards a superconducting joint between RE (rare earth) $Ba_2Cu_3O_{7-\delta}$-coated conductors *Supercond. Sci. Technol.* **28** 075010
[16] Ohki K *et al* 2017 Fabrication, microstructure and persistent current measurement of an intermediate grown superconducting (iGS) joint between REBCO-coated conductors *Supercond. Sci. Technol.* **30** 115017
[17] Mukoyama S, Nakai A, Sakamoto H, Matsumoto S, Nishijima G, Hamada M, Saito K and Miyoshi Y 2018 Superconducting joint of REBCO wires for MRI magnet *J. Phys.: Conf. Ser.* **1054** 012038
[18] Teranishi R, Hiramatsu K, Yasuyama S, Miyajima T, Sato Y, Kaneko K and Awaji S Matsumoto A and Inoue M 2019 Superconducting joint of $GdBa_2Cu_3Oy$ coated conductors by crystallization of an additionally deposited precursor layer *IEEE Trans. Appl. Supercond.* **29** 6602904
[19] Huang D, Shang H, Xie B, Zou Q, Dong H, Wang K, Zhang L, Gu H and Ding F 2022 An efficient approach for superconducting joint of YBCO coated conductors *Supercond. Sci. Technol.* **35** 075004
[20] Yanagisawa Y *et al* 2021 Development of a persistent-mode NMR magnet with superconducting joints between high-temperature superconductors *Supercond. Sci. Technol.* **34** 115006
[21] Kobayashi K, Nishijima G, Ohki K, Nagaishi T, Uchida A and Kitaguchi H 2022 In-field evaluation of REBCO superconducting joint *IEEE Trans. Appl. Supercond.* **32** 6601404
[22] Kim S B, Saito R, Takahashi M, Park Y J, Lee M H, Oh YK and Noguchi S 2016 Shape optimization of the stacked HTS double pancake coils for compact NMR relaxometry operated in persistent current mode *IEEE Trans. Appl. Supercond.* **26** 43017004
[23] Nishijima G, Matsumoto S, Nakai A, Sakamoto H, Mukoyama S, Miyoshi Y, Saito K and Hamada M 2019 Transport property of REBCO superconducting joints in magnetic fields at various temperatures *IEEE Trans. Appl. Supercond.* **29** 6602105
[24] Takeda Y, Nishijima G, Nakai U, Motoki T, Shimoyama J and Kitaguchi H 2023 Angular dependence of resistance and critical current of a Bi-2223 superconducting joint *Supercond. Sci. Technol.* **36** 125010
[25] Takeda Y, Nishijima G and Kitaguchi H 2025 Resistance and voltage–current characteristics of REBCO superconducting joint *IEEE Trans. Appl. Supercond.* **35** 6604106
[26] Kobayashi K, Nishijima G, Uchida A, Amaya M, Banno N and Kitaguchi H 2020 Development of a superconducting joint resistance evaluation system *IEEE Trans. Appl. Supercond.* **30** 9000204
[27] Senatore C, Barth C, Bonura M, Kulich M and Mondonico G 2016 Field and temperature scaling of the critical current density in commercial REBCO coated conductors *Supercond. Sci. Technol.* **29** 014002
[28] Francis A, Abraimov D, Viouchkov Y, Su Y, Kametani F and Larbalestier D C 2020 Development of general expressions for the temperature and magnetic field dependence of the critical current density in coated conductors with variable properties *Supercond. Sci. Technol.* **33** 044011
[29] Khan M R, Leo A, Masi A, Pinto V, Armenio A A, Augieri A, Celentano G, Martucciello N, Nigro A and Grimaldi G 2024 Characterization of critical fields and flux pinning energy of REBCO tapes *IEEE Trans. Appl. Supercond.* **34** 6602505
[30] Kato T, Yoshida R, Yokoe D, Ohki K, Nagaishi T, Yanagisawa Y, Hirayama T, Ikuhara Y and Maeda H 2020 Nanostructural evolution of intermediate grown superconducting joint layers between $GdBa_2Cu_3O_y$ coated conductors *Supercond. Sci. Technol.* **33** 105008
[31] Cai C, Holzapfel B, Hänisch J, Fernández L and Schultz L 2004 Magnetotransport and flux pinning characteristics in $RBa_2Cu_3O_{7-\delta}$ (R = Gd,Eu,Nd) and

$(Gd_{1/3}Eu_{1/3}Nd_{1/3})Ba_2Cu_3O_{7-\delta}$ high-Tc superconducting thin films on $SrTiO_3$(100) *Phys. Rev. B* **69** 104531
[32] Maiorov B, Baily S A, Zhou H, Ugurlu O, Kennison J A, Dowden P C, Holesinger T G, Foltyn S R and Civale L 2009 Synergetic combination of different types of defect to optimize pinning landscape using $BaZrO_3$-doped $YBa_2Cu_3O_7$ *Nat. Mater.* **8** 398–404
[33] Awaji S, Ishihara R, Watanabe K, Shikimachi K, Hirano N and Nagaya S 2011 Anisotropy of the critical current density and intrinsic pinning behaviors of $YBa_2Cu_3O_y$ coated conductors *Appl. Phys. Express* **4** 013101
[34] Miura M, Maiorov B, Baily S A, Haberkorn N, Willis J O, Marken K, Izumi T, Shiohara Y and Civale L 2011 Mixed pinning landscape in nanoparticle-introduced $YGdBa_2Cu_3O_y$ films grown by metal organic deposition *Phys. Rev. B* **83** 219901
[35] Long N J 2008 Model for the angular dependence of critical currents in technical superconductors *Supercond. Sci. Technol.* **21** 025007
[36] Roas B, Schultz L and Saemann-Ischenko G 1990 Anisotropy of the critical current density in epitaxial $Yba_2Cu_3O_x$ films *Phys. Rev. Lett.* **64** 1311
[37] Muto S, Fujita S, Iijima Y and Daibo M 2024 Evaluation and analysis of a 10 T-class small coil using REBCO coated conductors laminated with thick copper tapes *IEEE Trans. Appl. Supercond.* **34** 4603105
[38] Muto S, Fujita S, Nakamura N and Daibo M 2023 Evaluation and analysis of a 10T-class small coil using REBCO coated conductors laminated with thick copper tapes *MT-28 Int. Conf. on Magnet Technology (Aix-en-Provence, France)*
[39] Civale L *et al* 2004 Angular-dependent vortex pinning mechanisms in $YBa_2Cu_3O_7$ coated conductors and thin films *Appl. Phys. Lett.* **84** 2121–3
[40] Ohki K, Yamasaki H, Develos-Bagarinao K and Nakagawa Y 2008 Enhanced random pinning with oxygen annealing in YBCO films prepared by large-area pulsed laser deposition *Supercond. Sci. Technol.* **21** 045004
[41] Hilton D K, Gavrilin A V and Trociewitz U P 2015 Practical fit functions for transport critical current versus field magnitude and angle data from (RE)BCO coated conductors at fixed low temperatures and in high magnetic fields *Supercond. Sci. Technol.* **28** 074002
[42] Brittles G D, Mousavi T, Grovenor C R M, Aksoy C and Speller S C 2015 Persistent current joints between technological superconductors *Supercond. Sci. Technol.* **28** 093001
[43] Yamafuji K and Kiss T 1997 Current–voltage characteristics near the glass–liquid transition in high-T_c superconductors *Physica C* **290** 9–22
[44] Cai X Y , Polyanskii A, Li Q, Riley J G N and Larbalestier D C 1998 Current-limiting mechanisms in individual filaments extracted from superconducting tapes *Nature* **392** 906–9
[45] Jia Y, Hua J, Crabtree G W, Kwok W K, Welp U, Malozemoff A P, Rupich M and Fleshler S 2010 *C*-axis critical current density of second-generation YBCO tapes *Supercond. Sci. Technol.* **23** 115017
[46] Motoki T *et al* 2016 Microstructures and improved J_c–H characteristics of Cl-containing YBCO thin films prepared by the fluorine-free MOD method *Supercond. Sci. Technol.* **29** 015006
[47] Motoki T, Ikeda S, Honda G, Nagaishi T, Nakamura S and Shimoyama J 2017 Dramatic effects of chlorine addition on expanding synthesis conditions for fluorine-free metal–organic decomposition $YBa_2Cu_3O_y$ films *Appl. Phys. Express* **10** 023102
[48] Motoki T, Ikeda S, Nakamura S, Honda G, Nagaishi T, Doi T and Shimoyama J 2018 Greatly enhanced flux pinning properties of fluorine-free metal–organic decomposition YBCO films by co-addition of halogens (Cl, Br) and metals (Zr, Sn, Hf) *Supercond. Sci. Technol.* **31** 044004